Chemosphere 196 (2018) 575–584

Contents lists available at ScienceDirect

Chemosphere

journal homepage: www.elsevier.com/locate/chemosphere

Silver ion-enhanced particle-specific cytotoxicity of silver nanoparticles and effect on the production of extracellular secretions of *Phanerochaete chrysosporium*

Zhenzhen Huang [a, b], Piao Xu [a, b], Guiqiu Chen [a, b], Guangming Zeng [a, b, *], Anwei Chen [c, **], Zhongxian Song [d], Kai He [a, b], Lei Yuan [a, b], Hui Li [a, b], Liang Hu [a, b]

[a] College of Environmental Science and Engineering, Hunan University, Changsha, 410082, PR China
[b] Key Laboratory of Environmental Biology and Pollution Control (Hunan University), Ministry of Education, Changsha, 410082, PR China
[c] College of Resources and Environment, Hunan Agricultural University, Changsha, 410128, PR China
[d] School of Municipal and Environmental Engineering, Henan University of Urban Construction, Pingdingshan, 467036, PR China

HIGHLIGHTS

- Oxalate, MnP and LiP were obviously inhibited with the addition of Ag^+ into AgNPs.
- EPS can be used as carbon and energy sources by *P. chrysosporium* against toxicants.
- AgNPs-induced "particle-specific" toxicity was mainly ascribed to the added AgNPs.
- The cytotoxicity of AgNPs was enhanced with an increase in additional Ag^+ levels.

GRAPHICAL ABSTRACT

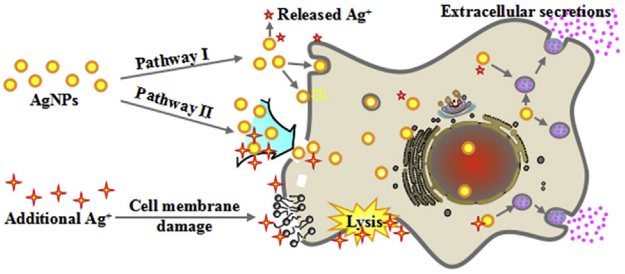

ARTICLE INFO

Article history:
Received 1 September 2017
Received in revised form
19 December 2017
Accepted 28 December 2017
Available online 30 December 2017

Handling Editor: Tamara S. Galloway

Keywords:
Silver nanoparticles
Silver ions
Phanerochaete chrysosporium
Extracellular secretions
Enhanced "particle-specific" cytotoxicity

ABSTRACT

This study investigated the influence of silver ions (Ag^+) on the cytotoxicity of silver nanoparticles (AgNPs) in *Phanerochaete chrysosporium* and noted the degree of extracellular secretions in response to the toxicant's stress. Oxalate production was elicited with moderate concentrations of 2,4-dichlorophenol (2,4-DCP) and AgNPs reaching a plateau at 10 mg/L and 10 μM, respectively. Increased oxalate accumulation was accompanied by higher activities of manganese peroxidase (MnP) and lignin peroxidase (LiP). However, the secretion of oxalate, MnP and LiP was significantly inhibited owing to Ag^+ incorporation into AgNP solution. Production of extracellular polymeric substances (EPS) significantly elevated with an increase in 2,4-DCP concentrations; however, after 24 h of exposure to 100 mg/L 2,4-DCP, an obvious decrease in EPS occurred, indicating that part of EPS could be consumed as carbon and energy sources to ameliorate biological tolerance to toxic stress. Furthermore, AgNP-induced "particle-specific" cytotoxicity was substantially enhanced with additional Ag^+ as evidenced by its significant negative impact on cellular growth, plasma membrane integrity, and morphological preservation compared with AgNPs at equal Ag concentration.

1. Introduction

Silver nanoparticles (AgNPs) have attracted immense attention in various domains particularly in physical sciences, technology,

* Corresponding author. College of Environmental Science and Engineering, Hunan University, Changsha, 410082, PR China.
** Corresponding author.
E-mail addresses: zgming@hnu.edu.cn (G. Zeng), A.Chen@hunau.edu.cn (A. Chen).

https://doi.org/10.1016/j.chemosphere.2017.12.185
0045-6535/

biomedicine, and pharmacy owing to their exceptional photoelectronic, photocatalytic, and chemical properties (Krystosiak et al., 2017; Yuan et al., 2016; Zhang et al., 2015). Silver salts (mostly silver nitrate) are also renowned for their broad-spectrum antimicrobial activity. Silver and silver salts are expected to find their way into aquatic environments during various stages of production, medical application, and waste disposal, resulting in increased risk to human health and adverse impacts on microbes in the environment and biological wastewater treatments (Girilal et al., 2015; Sheng and Liu, 2017; Zeng et al., 2013a; Xu et al., 2012). Generally, AgNP toxicity, the degree of which is associated with the oxidative dissolution rate of AgNPs, is partly attributed to the released Ag^+ (Zuo et al., 2015; He et al., 2014). However, substantial evidences have demonstrated that AgNPs can execute direct particle effects or both ion and particle effects in complex systems as well as in simple systems. For example, AgNPs exerting direct "particle-specific" effects exhibited robust cytotoxicity to RNA polymerase, and both Ag^+ and AgNPs simultaneously incurred biological influences on erythroid cells (Wang et al., 2013). Similarly, AgNPs were documented to induce a "Trojan-horse" effect during the degradation process of 2,4-dichlorophenol (2,4-DCP) by *Phanerochaete chrysosporium* (*P. chrysosporium*), and the synergistic effect of AgNPs and microbes was observed (Huang et al., 2017). Besides, studies on the combined toxic effects of AgNPs and other substances such as antibiotics and Ag^+ on bacteria have been reported (Wang et al., 2016). Combination of AgNPs and Ag^+ led to difference in the time of event occurrence and consequent responsive cascades (Mendes et al., 2015). Although antagonism in the coexistence of AgNPs and additional Ag^+ influenced the generation of hydroxyl radical (He et al., 2012), the possible mechanism of this combined effect and the scale of toxicity attributable to just the AgNPs are still under investigation. Therefore, to gain better insight into the bioeffects and risk associated with AgNPs, it is necessary to explore the mechanism of the combined effects of AgNPs and additional Ag^+.

It is noteworthy that bioremediation is considered as a highly promising technique in the removal of heavy metals and organic pollutants, owing to its cost-effectiveness, environmental compatibility, and operational efficiency (He et al., 2017; Fan et al., 2008; Cheng et al., 2016). Nevertheless, cellular growth, morphology, and biochemical activities of the microbes are adversely affected because of the biotoxicity of contaminants, leading to a decrease in biomass and treatment capacity, and a limitation to popularization and development of biological technologies (Chen et al., 2015; Yang et al., 2010). *P. chrysosporium*, as the model species of white-rot fungi, has been widely used in the removal of various heavy metals through intracellular bioaccumulation and the binding of mycelium and extracellular polymeric substances (EPS). EPS consist of lipids, proteins, polysaccharides, humic substances, and other polymeric compounds (Chen et al., 2015; Huang et al., 2015b), and their molecules comprise functional groups such as amino, amide, hydroxyl, carboxyl, and phosphoryl, which contribute to the detoxification of heavy metals (Sheng et al., 2013; Yue et al., 2015). Furthermore, oxalic acid, another extracellular secretion, can immobilize soluble metal ions as metal-oxalate crystals, which play a crucial role in heavy metals tolerance in oxalic acid-secreting fungi (Xu et al., 2015). Meanwhile, *P. chrysosporium* can degrade and transform organic pollutants, such as 2,4-DCP with low biodegradability, potential mutagenicity, carcinogenicity, and highly toxic effects on both microorganisms and humans (even at a very low level) (Zhan et al., 2017; Barik and Gogate, 2017; Tang et al., 2008), through an array of extracellular ligninolytic enzymes, including lignin peroxidase (LiP), manganese peroxidase (MnP), and a copper-containing phenoloxidase known as laccase (Lac) (Huang et al., 2016).

Previous studies were primarily focused on the removal of AgNPs and 2,4-DCP from aqueous solutions, and their toxic effects on mycelia morphology, growth, reproduction of fungi, and enzyme activities under stress (Zuo et al., 2015; Huang et al., 2017). However, information on the responses of extracellular secretions to simultaneous AgNP and 2,4-DCP challenge is unavailable. Furthermore, an understanding of the mechanism of AgNP toxicity in the fusion of AgNPs and additional Ag^+ is essential. Therefore, the present study aimed at unraveling the behavior of extracellular secretions and the molecular mechanisms of AgNP toxicity in *P. chrysosporium* under the combined stress of AgNPs and additional Ag^+. Real-time changes with regard to oxalate, MnP, LiP, Lac, mycelial dry biomass, EPS, and extracellular proteins of *P. chrysosporium* at different concentrations of 2,4-DCP, AgNPs, and/or Ag^+ were investigated. In addition, analyses of scanning electron microscopy (SEM), scanning transmission electron microscopy (STEM) equipped with an energy-dispersive X-ray (EDX) attachment in high-angle annular dark field (HAADF) mode, and X-ray diffraction (XRD) facilitated the elucidation of potential detoxification roles of extracellular secretions and a mechanistic understanding of AgNP toxicity.

2. Material and methods

2.1. Strain cultivation and treatments

P. chrysosporium BKMF-1767 (CCTCC AF96007) obtained from the China Center for Type Culture Collection was maintained on potato dextrose agar plates at 4 °C. After cultivation for 3 days, *P. chrysosporium* pellets were rinsed three times with 2 mM Na_2HCO_3 buffer solution and then exposed to treatments of 2,4-DCP, AgNPs, and/or Ag^+. Detailed descriptions on the treatments can be found in Supporting Information. The mycelia and culture solutions were harvested for further analysis. Citrate-stabilized AgNPs were synthesized according to our previous method (Huang et al., 2017). Zeta potentials of the tested solutions exposed to AgNPs/Ag^+ separately and in combination were determined using a Malvern Zetasizer Nano ZS. All the chemicals used were at least of analytical reagent grade and purchased from Sigma-Aldrich and Aladdin.

2.2. Assessment of extracellular secretions, cellular survival, and membrane integrity

Analysis of oxalate in the culture medium was implemented by using high performance liquid chromatography (HPLC, Agilent 1100). The activities of MnP and LiP in the extracellular medium were measured according to Chen et al. (2015). Lac activity was assayed by spectrophotometrically monitoring the oxidation of ABTS at 420 nm (Huang et al., 2016). EPS secreted by *P. chrysosporium* were preliminarily quantified according to the phenol-sulfuric acid assay using glucose as standard (Li et al., 2015). Extracellular protein content was determined via Bradford method with a UV–visible spectrophotometer at 595 nm (Huang et al., 2017). Cellular survival after exposure to AgNPs and/or Ag^+ was assessed according to our previous study and expressed as a relative percentage to the control treated with nothing (Chen et al., 2015). Membrane integrity of cells treated with 2,4-DCP, AgNPs and/or Ag^+ was determined by using the fluorescent dye propidium iodide (PI) (Chen et al., 2014). All experiments were performed in triplicate and data were analyzed with SigmaPlot 12.0 and Origin 9.0 software.

Detailed measurements of oxalate production, ligninolytic enzyme activity, EPS quantification, and membrane integrity are supplied in Supporting Information.

3. Results and discussion

3.1. Oxalate production

Oxalate has been reported to be one of the primary and important metabolites with elaborated responses to the stress of toxic metals and organic pollutants in *P. chrysosporium* (Huang et al., 2008, 2015a). Oxalate accumulations increased with an increase in 2,4-DCP concentration reaching a plateau (1.63 mM) at 10 mg/L; however, further elevation in the concentration of 2,4-DCP to 100 mg/L resulted in a significant decline in oxalate production (Fig. 1A). This suggested that higher concentration of oxalate production was induced by an appropriate addition of 2,4-DCP, which probably ameliorated the carbon and energy supplying system and further contributed to the biosynthesis of oxalate by oxaloacetase and glyoxylate oxidase (Xu et al., 2015; Li et al., 2011). Besides, it is noteworthy that oxalate concentrations in the control were higher than those in the samples treated with 0, 50, 75, and 100 mg/L 2,4-DCP in the first 60 h. However, after 60 h of exposure, a subsequent decrease in oxalate concentration occurred in the control samples, possibly indicating the degradation of oxalate (Li et al., 2011).

As shown in Fig. 1B, two plateaus were observed during the processes of AgNP-induced oxalate production. The first maximum oxalate accumulation (1.25 mM) was detected after 12 h in the extract without AgNPs but including 25 mg/L 2,4-DCP (0 μM AgNPs), indicating that oxalate secretion was promoted by low concentrations of 2,4-DCP. A similar phenomenon was observed when comparative treatments of 1 μM Ag^+ with and without 2,4-DCP were performed (Fig. 1C). Then, oxalate production in the medium increased with increased exposure time and attained another peak value at 84–96 h (Fig. 1B). The peak values of oxalate production were 0.90, 1.35, 1.11, 0.82, and 0.72 mM at AgNPs concentrations of 0, 10, 30, 60 and 100 μM, respectively. Oxalate accumulations beyond 24 h of exposure to AgNPs were similar to those under 2,4-DCP stress, which implied that the appropriate AgNP concentration could also promote oxalate biosynthesis.

Furthermore, higher secretion of oxalate was possibly because of higher oxalate consumption for extracellular chelation of heavy metals. Organic acids (e.g., oxalic, lactic, fumaric, and malic acids) chelating metals were regarded as important tolerance mechanisms (Xu et al., 2015; Huang et al., 2008). It was found that oxalate production contributed to the detoxification of heavy metals via chelating and immobilizing them in *P. chrysosporium* (Li et al., 2011). Release of oxalate typically participated in extracellular sequestration or precipitation of cations via the formation of insoluble oxalate crystals. In comparison with Ag^+, AgNPs and 2,4-DCP can stimulate oxalate secretion by *P. chrysosporium* to a greater extent (Fig. 1). We have previously found that the synergistic effects of AgNPs on 2,4-DCP degradation in the presence of *P. chrysosporium* contributed to oxalate production during the processes of 2,4-DCP degradation and fungal metabolism (Huang et al., 2017). This may be another reason for higher levels of oxalate induced by AgNPs and 2,4-DCP.

Additionally, AgNP treatment resulted in a significant increase in oxalate at 10 μM (Fig. 1C). However, negligible difference in oxalate production was found among 1 and 10-μM Ag^+ exposure alone and the combined exposure to 10 μM AgNPs and 1 μM Ag^+. The findings indicated that the secreted amount of oxalate was significantly affected as a result of the incorporation of Ag^+ into AgNPs.

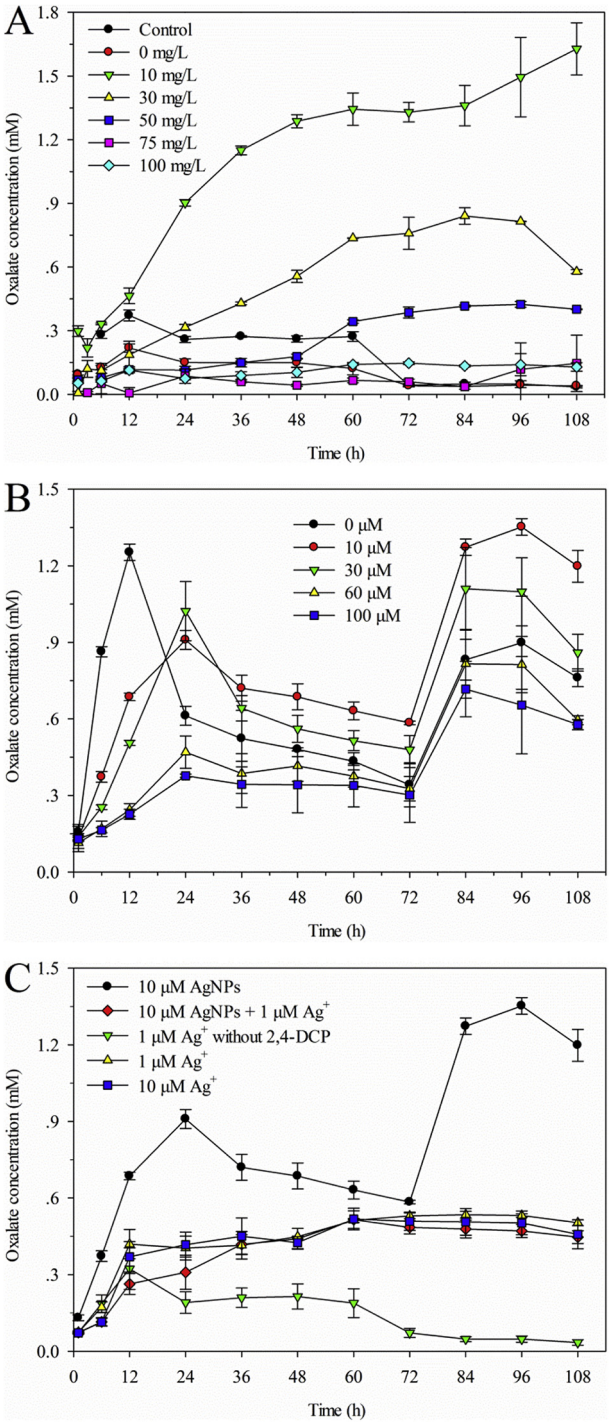

Fig. 1. Oxalate concentrations of *P. chrysosporium* exposed to diverse concentrations of (A) 2,4-DCP, (B) AgNPs, and (C) Ag^+ as well as 10 μM AgNPs + 1 μM Ag^+.

3.2. Ligninolytic enzyme activities

3.2.1. MnP activity

MnP, the most common lignin-modifying peroxidase, can be produced by almost all white-rot fungi (Huang et al., 2015a). Changes in MnP activity after exposure to various concentrations of 2,4-DCP, AgNPs, and/or Ag^+ are presented in Fig. 2. MnP activity was time- and concentration-dependent during the entire degradation process of 2,4-DCP. Two peaks were revealed in the patterns of MnP activities in the 2,4-DCP-treated groups, the first peak at 6–12 h and the second at 60 h (Fig. 2A). The maximum activities of MnP were 2.00 U/L in the control and 2.75, 4.19, and 3.44 U/L in the groups exposed to 0, 50, and 100 mg/L 2,4-DCP, respectively. More

importantly, MnP activities under 2,4-DCP stress were higher than those in the control throughout the exposure period. The phenomenon indicated that *P. chrysosporium* might maintain excellent MnP activities under 2,4-DCP stress, which was mainly attributed to the 2,4-DCP-resistant character of *P. chrysosporium* (Huang et al., 2015b, 2017). Similar results about the excellent tolerance profile of *P. chrysosporium* to phenol were also reported (Huang et al., 2015a).

Similarly, MnP activities under AgNP stress at concentrations of 0, 10, 30, 60, and 100 μM showed the maximum values (5.29, 5.47, 7.29, 4.81, and 4.02 U/L, respectively) at 6 or 60 h (Fig. 2B). Higher activities of MnP were recorded within 60 h of exposure to 0–60 μM AgNPs, while a low MnP activity was observed in response to 100-μM AgNP treatment over the same exposure period. The increased MnP activity was probably due to low AgNP concentrations positively affecting the activity and stability of the enzyme (Hatvani and Mécs, 2003), further enhancing fungal metabolism to maintain energy in response to AgNP exposure (Huang et al., 2010). Besides, high levels of MnP activities were detected together with high oxalate concentrations under AgNP exposure (Figs. 1b and 2b). It was in agreement with previous findings of Li et al. (2011) who reported a positive correlation between MnP activity and oxalate concentration in the enzymatic cycle of fungi. Therefore, another possibility was that MnP activity could be stimulated by the increasing concentration of oxalate, which generated diffusible oxidizing chelates to stabilize Mn^{3+} (Zeng et al., 2010; Li et al., 2011; Huang et al., 2015a). However, addition of 100 μM of AgNPs decreased MnP activity, probably because of the alteration in microbial physiology after excessive AgNP exposure. The Mn-binding sites in MnP are flexible to bind a wide variety of metal ion. Accordingly, another possible explanation was that MnPI and MnPII reduction processes were inhibited by high doses of AgNPs, leading to the inhibition in MnP (Xu et al., 2015). Interestingly, highly active MnP was resumed in response to 100-μM AgNP treatment for 72–96 h, which might be due to the lowering of soluble/exchangeable levels of Ag in the solution (Huang et al., 2010).

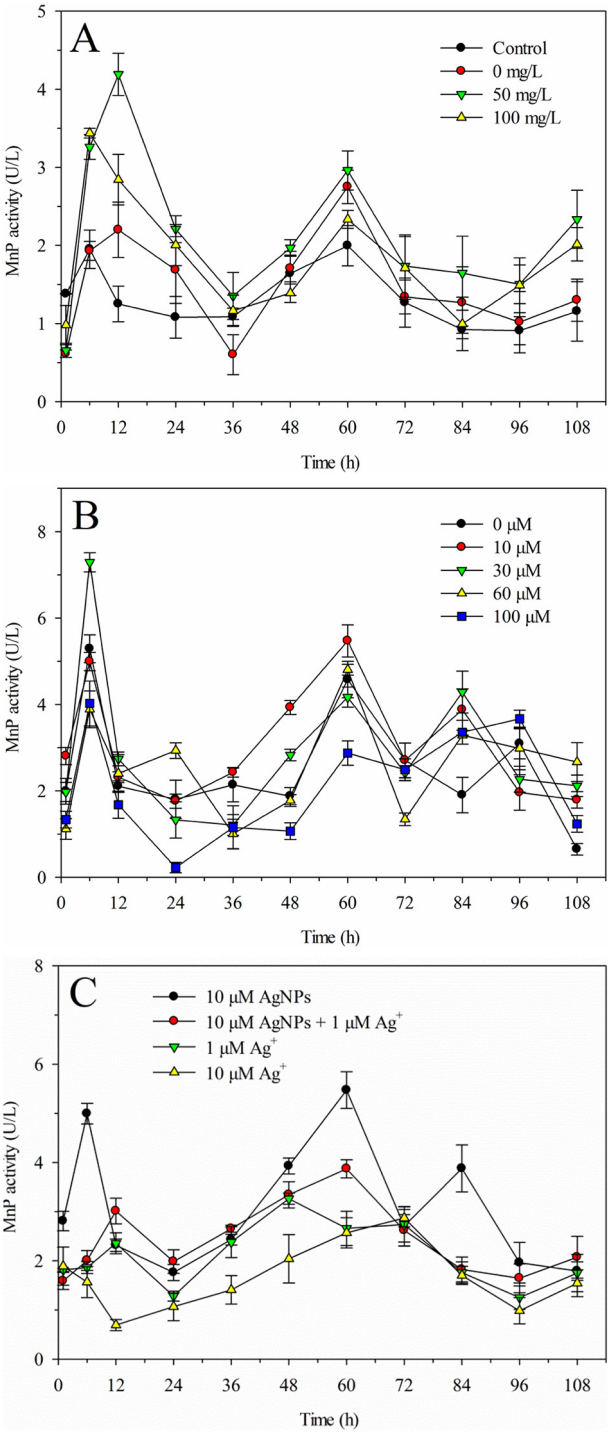

Fig. 2. Variation of MnP activity of *P. chrysosporium* treated with different concentrations of (A) 2,4-DCP, (B) AgNPs, and (C) Ag^+ as well as 10 μM AgNPs + 1 μM Ag^+.

As shown in Fig. 2C, MnP remained high in the 10 μM AgNP-treated group almost throughout the entire process. In contrast, it was relatively low in 1 and 10 μM Ag^+-treated groups. This suggested that Ag^+ exerted considerably higher toxicity than AgNPs did. The combined treatment with 1 μM Ag^+ and 10 μM AgNPs resulted in low MnP activities as well. The combined effect was consistent with the result of the oxalate secretion.

3.2.2. LiP activity

Variations in LiP activities under 2,4-DCP, AgNP, and/or Ag^+ stress are shown in Fig. 3. The maximum LiP activities achieved after 72 h were 6.69 U/L in control and 6.45, 4.95, and 5.09 U/L in the groups exposed to 0, 50, and 100 mg/L 2,4-DCP, respectively (Fig. 3A). Besides, LiP levels in 50 and 100 mg/L 2,4-DCP treatment groups were markedly lower than those in the control group and 0 mg/L 2,4-DCP treatment group within 72 h, especially at 12 and 60 h. This result suggested that the activity of LiP can be suppressed by 2,4-DCP to some extent. However, as mentioned above, 2,4-DCP elicited high levels of MnP with respect to the control. Consequently, LiP was more sensitive to phenol compared with MnP. Furthermore, the time for LiP activity to reach its peak was slightly longer than that for MnP. This time difference may be due to the fact that LiP production depends on hydrogen peroxide (H_2O_2) formation via MnP oxidation of oxalate (Li et al., 2011). Thus, the production of LiP and MnP was closely related with oxalate accumulation.

A significant stimulation in LiP activity was observed at low doses of AgNPs and the maximum value (6.64 U/L at 24 h) was reached with 30 μM AgNPs (Fig. 3B). Conversely, a decrease in LiP activity was detected when the initial concentrations of AgNPs were higher than 30 μM. These findings indicated that low levels of AgNPs elicited increased production of ligninolytic extracellular enzymes (LiP and MnP). Cellular repair mechanisms against toxicants were activated under low-dose exposure, leading to overcompensatory responses to AgNP stress (Zuo et al., 2015; Huang et al., 2017), which could be the reason why low-concentration stimulation led to highly active ligninolytic enzymes. Nevertheless, the greater inhibition in LiP activity noted with a higher

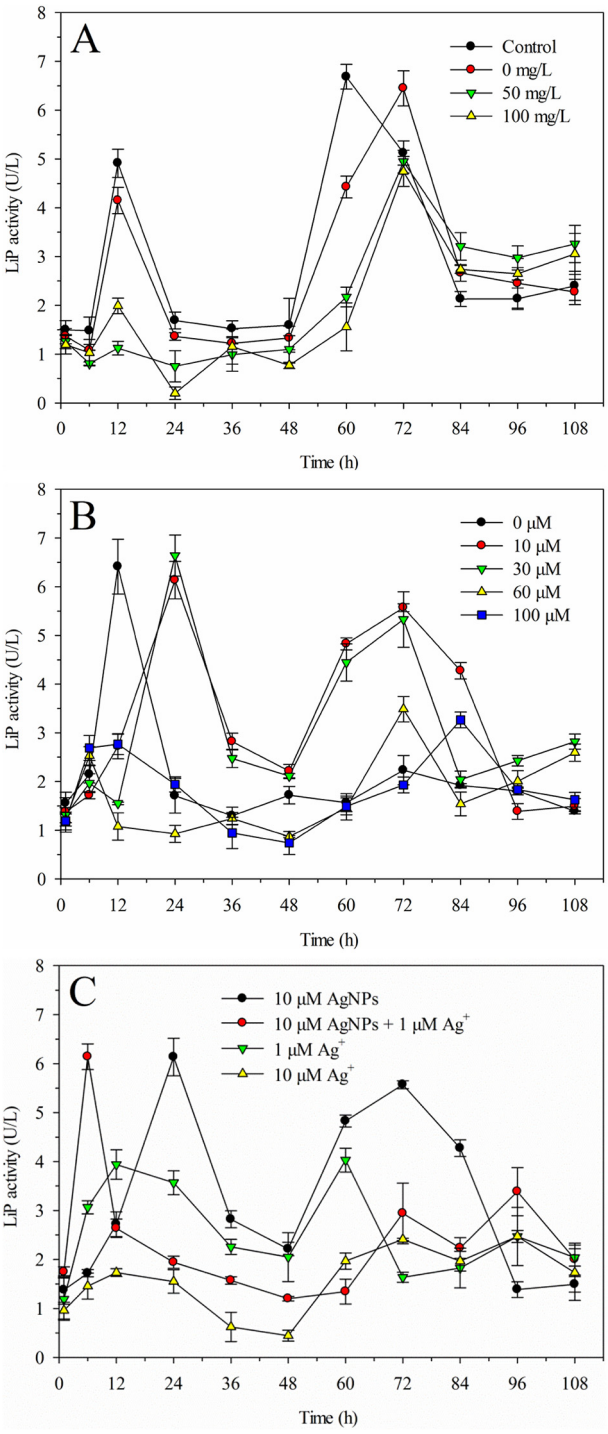

Fig. 3. Variation of LiP activity of *P. chrysosporium* treated with different doses of (A) 2,4-DCP, (B) AgNPs, and (C) Ag^+ as well as 10 μM AgNPs + 1 μM Ag^+.

concentration of AgNPs might be because enzyme production was disturbed at transcriptional and translational regulation levels after their entering fungal cells (Huang et al., 2010).

As shown in Figs. 2C and 3C, treatment with 1 μM Ag^+ displayed higher activities of MnP and LiP than those with 10 μM Ag^+ during the whole incubation period, which suggested that high Ag^+ concentrations can depress MnP and LiP activities. In addition, although the maximum LiP level for 10 μM AgNPs treatment (6.14 U/L) was equal to that for the combined treatment of 10 μM AgNPs and 1 μM Ag^+, higher levels of LiP were observed under single AgNP stress after more than 12 h (Fig. 3C). It can be speculated that the addition of Ag^+ resulted in increased cytotoxicity in the presence of AgNPs, further inhibiting the activity of LiP. The result was consistent quite well with oxalate production and MnP activity measurements.

Similarly, Lac activity varied with exposure time and concentrations of 2,4-DCP, AgNPs, and/or Ag^+ (Fig. S1). However, Lac played only a minor role in the resistance to the external stress, relative to fungal peroxidases LiP and MnP. A detailed description is available in the Supporting Information.

3.3. EPS production

The quantity of EPS in *P. chrysosporium* was measured in the groups treated with various concentrations of 2,4-DCP, AgNPs, and/or Ag^+. An increase in EPS was observed with increasing 2,4-DCP concentrations from 0 to 100 mg/L (Fig. 4A). The highest amounts of EPS achieved at 24 h were 22.4, 20.0, 37.9, and 75.8 mg/L at 2,4-DCP concentrations of 0, 25, 50, and 100 mg/L, respectively, which were higher than that of control (14.9 mg/L). EPS production was boosted to possibly cope with toxicant-induced oxidative stress, and positively correlated with tolerance to the pollutant as indicated in previous reports (Chen et al., 2015). Furthermore, the higher quantities of EPS in the 100 mg/L 2,4-DCP-treated group (Fig. 4A) may also have originated from lysis because of adverse influence on cellular growth (Li et al., 2015). There was no significant change in the amount of EPS after exposure to low concentrations of 2,4-DCP (≤50 mg/L) over 48 h; however, EPS production decreased continually under 100 mg/L 2,4-DCP stress. This suggested that the exposure to low concentrations of 2,4-DCP, which can be exploited as carbon and energy sources by *P. chrysosporium* for its proliferation (Huang et al., 2017), led to a rapid recovery of metabolic function to near original levels in EPS (Xiu et al., 2012). Although a high concentration of 2,4-DCP is highly toxic to cells, parts of EPS could be also reutilized by *P. chrysosporium* as a source of carbon and energy to ameliorate its biological functions and stress resistance in the case of starvation or malnutrition (Shi et al., 2017).

When *P. chrysosporium* pellets were treated with various concentrations of AgNPs, EPS production dropped with an increase in AgNP concentration, but changed a little beyond 48 h (Fig. 4B) probably due to Ag removal (including Ag^+ and AgNPs) reaching an equilibrium state at that time (Huang et al., 2017). EPS could adsorb and store nutrients for enhancement in cellular growth and adhesion and provide a protective barrier against external stresses, especially for the alleviation of toxicity of metal and metal oxide nanoparticles via their abundant metal-binding sites (Chen et al., 2014; Li et al., 2016). The binding of AgNPs to EPS resulted in lower AgNP bioavailability and subsequent toxicity, which in turn affected the secretion of EPS. AgNP exposure was also shown to be detrimental to the production of EPS in activated sludge (Geyik and Çeçen, 2016).

As shown in Fig. 4C, no distinct change in EPS concentrations was detected in the supernatants inoculated with 10 μM AgNPs and 1 μM Ag^+ separately and in combination. However, exposure to 10 μM Ag^+ alone and the combination of 10 μM AgNPs and 10 μM Ag^+ resulted in maximum and minimum EPS productions, respectively. The difference between AgNP and Ag^+-induced phenomena was possible because increased EPS production protected fungal cells against the higher toxicity of Ag^+ compared with AgNPs. EPS had a higher affinity for AgNPs than to Ag^+, and the AgNP-EPS complexes reduced the bioavailability and potential toxicity of AgNPs, leading to low levels of EPS, which was another likely reason (Geyik and Çeçen, 2016; Chen et al., 2011). In contrast,

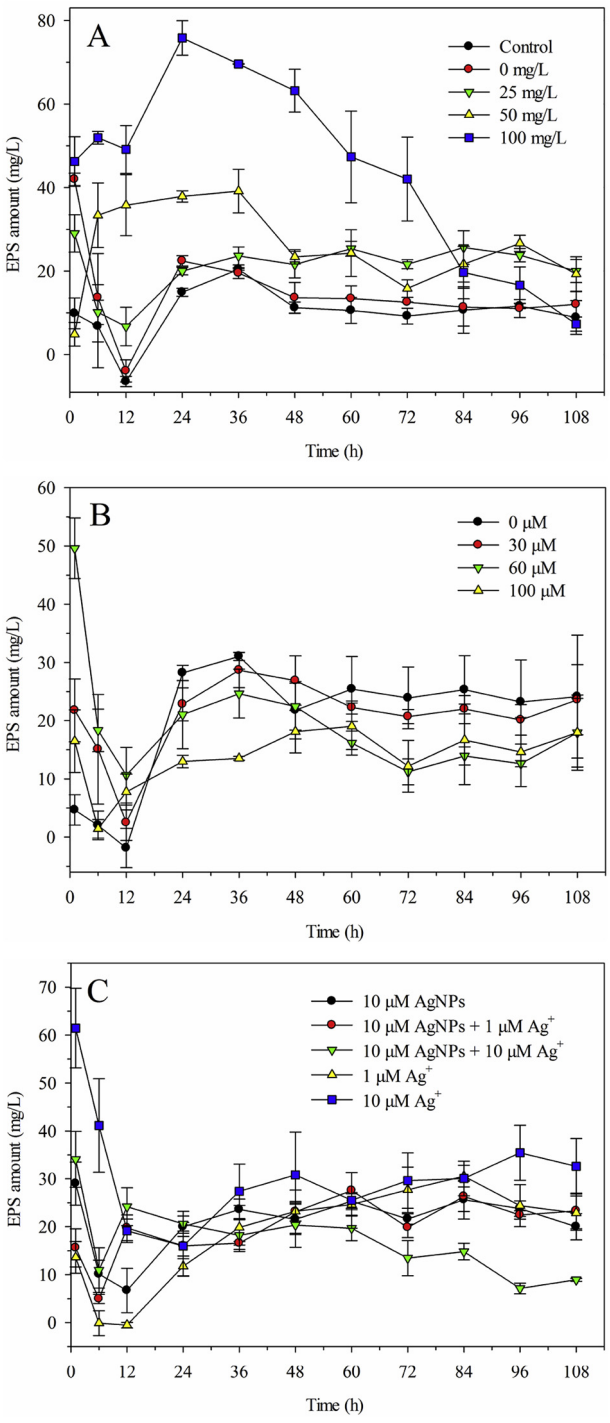

Fig. 4. EPS production of *P. chrysosporium* after exposure to various concentrations of (A) 2,4-DCP, (B) AgNPs, and (C) Ag^+ as well as AgNPs + Ag^+.

less EPS accumulation in the samples exposed to the combination of 10 μM AgNPs and 10 μM Ag^+ could be attributed to the fact that EPS was indeed consumed by *P. chrysosporium* to protect its cells against apoptosis and that the consumption rate exceeded its production rate.

3.4. Extracellular protein content

Variations in extracellular proteins secreted by *P. chrysosporium* were investigated, fluctuating with exposure time and concentrations of 2,4-DCP, AgNPs, and Ag^+ (Fig. 5). Extracellular protein production was remarkably promoted under a high concentration of 2,4-DCP stress (100 mg/L), while low levels of 2,4-DCP (0–50 mg/L) had insignificant stimulatory effects on extracellular protein content (Fig. 5A). The observation was similar to that for EPS. However, different patterns of changes in extracellular proteins (approaching equilibrium) and EPS (gradual decrease) were observed at 100 mg/L 2,4-DCP, indicating that EPS composition underwent changes, making it a potential source of carbon and energy, rather than nitrogen, which resulted in partial EPS degradation.

When the tested solutions contained 10 μM AgNPs, a slight increase in extracellular protein was induced with 1 μM Ag^+ addition, while 10 μM Ag^+ incorporation gave rise to an obvious stimulatory effect on extracellular protein secretion (Fig. 5B). This may be due to a defense response of *P. chrysosporium* against the toxicity of AgNPs and Ag^+. Proteins have been shown to bind to nanoparticles via cysteine residues, amine groups, or negatively charged carboxylate groups present in microorganisms, and the carboxyl groups of peptides and amino acid residues have a strong binding and stabilization ability to metal ions (Chen et al., 2011). In addition, greater differences were noticed in extracellular protein content compared with our previous study (Huang et al., 2017), which was probably because the used *P. chrysosporium* stemmed from

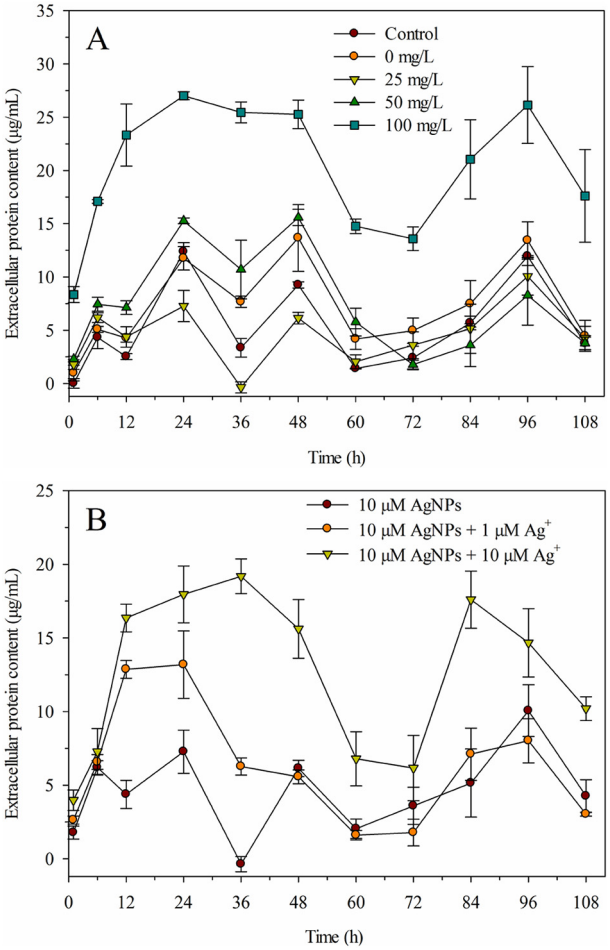

Fig. 5. Extracellular protein content of *P. chrysosporium* after treatments with different concentrations of (A) 2,4-DCP, (B) the single and combined treatments with AgNPs and Ag^+.

different batches of spores and different storage periods. Fungal spores used in our previous study were fresher than those used in the present study, and their storage period in the former was shorter than that in the latter. Extracellular proteins can be remarkably stimulated by high doses of AgNPs, rather than Ag^+, as also found previously (Huang et al., 2017). Combining the observation of high-dose Ag^+ incorporation into AgNPs and AgNP-induced stimulation in extracellular protein, it was hypothesized that the combination of AgNPs and Ag^+ resulted in negative impacts on extracellular oxidative systems, further influencing the secretions of extracellular proteins. This speculation was likewise extrapolated to other extracellular secretions, such as oxalate, MnP, and LiP. These results could be related to the influence of the introduction of Ag^+ on AgNP cytotoxicity. Subsequent analysis was focused on synergistic toxic effects of AgNPs and Ag^+ to *P. chrysosporium* and their mechanisms from four aspects: cellular growth, plasma membrane damage, morphological characteristics, and the pathway of cytotoxicity induced by AgNPs.

3.5. Cellular growth

Growth of *P. chrysosporium* was inhibited by high levels of 2,4-DCP and Ag^+, and Ag^+ elicited significantly greater cytotoxicity to *P. chrysosporium* than AgNPs did (Fig. S2). Besides, the combination of AgNPs and Ag^+ exhibited similar cytotoxicity effects on cellular growth to single AgNPs compared with single Ag^+. It may be speculated that AgNPs exerted cellular toxicity possibly through a "particle-specific" pathway, namely by nanoparticles themselves, rather than dissolved Ag^+, in the complex system. Detailed descriptions on cellular growth are available in Supporting Information.

3.6. Membrane damage

To examine membrane integrity under toxicant stress, the plasma membrane of *P. chrysosporium* was stained evenly with PI. Stronger red fluorescence was shown when *P. chrysosporium* cells were exposed to 100 mg/L 2,4-DCP and 100 μM AgNPs compared with control (Fig. 6A, F and G). Apparently, membrane integrity was extremely damaged by high concentrations of toxicants. It was noteworthy that *P. chrysosporium* cells showed weaker red fluorescence after exposure to single and combined treatments with 10 μM AgNPs and 1 μM Ag^+ than those challenged with 10 μM AgNPs and 10 μM Ag^+ simultaneously (Fig. 6B–E). This implied that high-level exposure to Ag^+ triggered a loss of membrane integrity. Coupled with the observations regarding EPS and extracellular proteins, PI staining assay showed that the addition of high-level Ag^+ in the presence of AgNPs led to obvious cell damage and even death. It can be assumed that additional Ag^+ exposure in a concentration-dependent manner promoted the uptake of AgNPs/Ag^+ and increased their toxicity to *P. chrysosporium*. To validate the hypothesis, combined cytotoxicity of AgNPs and Ag^+ was explored, and the findings are presented in the following section.

3.7. Association of Ag^+ with AgNP cytotoxicity

3.7.1. Combined effects of Ag^+ and AgNPs on the survival of *P. chrysosporium*

Survival rates of *P. chrysosporium* exposed to Ag^+ and AgNPs were measured to quantitatively investigate their combined cytotoxicity (Fig. S3). AgNPs alone (10 and 20 μM) and Ag^+ alone with a concentration of 1 μM enhanced the survival of the tested fungi compared with control. However, the combination of Ag^+ and AgNPs indeed led to a decline in survival rates of *P. chrysosporium*. After introduction of Ag^+, even at a concentration of 1 μM, 10 μM AgNPs can inhibit significantly the survival of *P. chrysosporium* by 82%. When Ag^+ concentration was 10 μM, the microbial survival rates were 68% and 62% in the presence and absence of AgNPs, respectively, which possibly implied that Ag^+ mainly contributed to cytotoxicity. Besides, around 74% of the tested fungi were killed by 20 μM Ag^+ alone. Although identical concentration of Ag (20 μM) was applied, Ag^+ alone showed a higher killing effect on *P. chrysosporium* than AgNPs alone and AgNPs combined with Ag^+. It was verified once again that Ag^+ exhibited significantly greater cytotoxicity compared with AgNPs.

3.7.2. SEM analysis

To gain further insight into the association between Ag^+ and AgNP cytotoxicity, different levels of Ag^+, i.e. 1 and 10 μM, were added into the tested medium containing AgNPs. SEM micrographs of the surfaces of 1 μM Ag^+-treated fungus with and without 10 μM AgNPs appeared clean and smooth with a large amount of void spaces, whereas fungal hyphae were widened following the combined treatment with AgNPs and Ag^+ (Fig. 7A). This indicated that low-level incorporation of Ag^+ into AgNPs evoked changes in microbial growth and metabolism, to a lesser extent, which was also be reflected by the aforementioned observations of the extracellular secretions. However, the analysis of 10 μM Ag^+ treatment showed an image of matted mycelia with denser extracellular deposits than that with the combined treatment with 10 μM AgNPs and 10 μM Ag^+ (Fig. 7B). It further implied that high levels of Ag^+ induced more severe toxicity to *P. chrysosporium* than AgNPs at equal Ag concentration. Coupled with the results regarding EPS and extracellular proteins, the extracellular deposits adhering to mycelial surfaces were formed in response to external stresses and potentially contained extracellular proteins. Taken together, AgNPs were found to have more pronounced effects on cell structures accompanied by more serious damage following exposure to Ag^+, which could be explained by that the attachment of AgNPs to the fungal surface and the uptake of bioavailable silver were enhanced in the presence of Ag^+.

In our study, the synergistic toxicity of AgNPs and Ag^+ disrupted plasma membrane integrity of fungal cells and exacerbated their morphological structures compare with that of single AgNPs. There was a possibility of the adsorption of Ag^+ onto negatively charged AgNPs. The observation was consistent with the previous studies that physical contact between AgNPs and microbial cell walls may give rise to damage to plasma membrane integrity and interaction of AgNPs with negatively charged bacterial membranes can be modulated by surface charges of AgNPs. It has also reported that Ag^+ can adhere to AgNP surfaces (Wang et al., 2016). In this study, after introduction of Ag^+, the subsequent surface charge of AgNPs indeed tended to move forward in a more positive direction (Table 1), resulting in the adherence of AgNPs to negatively charged fungal strains with higher probability. The improved attachment of AgNPs to fungus induced by Ag^+ might contribute to AgNPs/Ag^+ delivered into cells more effectively, further increasing their cytotoxicity. It was speculated that AgNPs and Ag^+-AgNP complexes crossed the cell membranes and biological barriers mainly through two pathways: a free shuttle (endocytosis or micropinocytosis, Pathway I), and the damaged parts of membranes (Pathway II). Furthermore, the delivery of AgNPs and Ag^+-AgNP complexes into cells could also enhance the internalization potential of Ag^+ (released Ag^+ and additional Ag^+ using $AgNO_3$ as Ag^+ source).

3.7.3. STEM-EDX and XRD analyses

AgNP (10 μM)-treated mycelial pellets (with or without 1 and 10 μM Ag^+) were analyzed via STEM in HAADF mode to reveal the enhanced Ag^+-induced toxicity of AgNPs and the mechanisms in *P. chrysosporium*. Nanoscale spherical particles (bright dots) can be

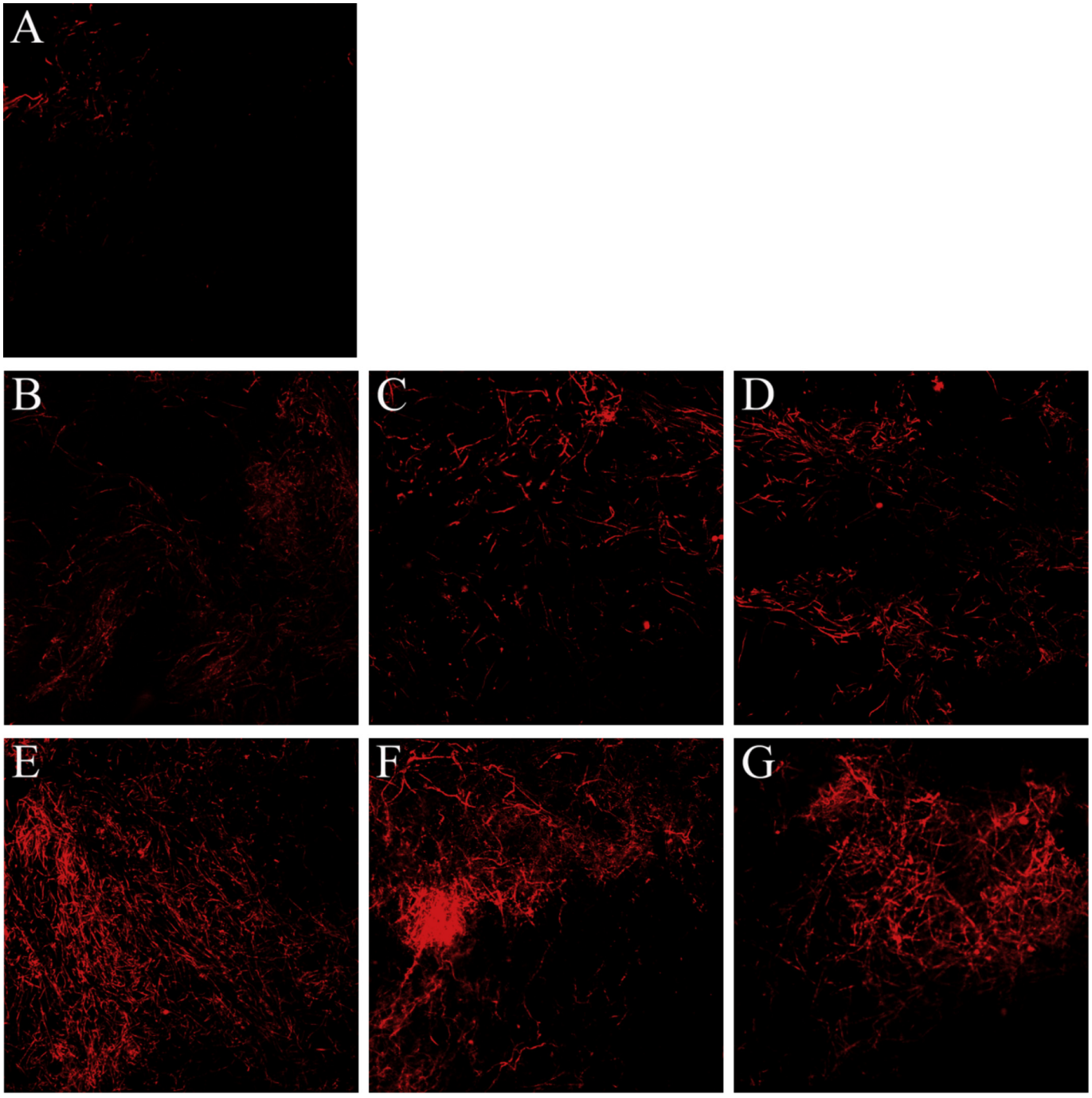

Fig. 6. Fluorescence images reflecting the plasma membrane integrity of *P. chrysosporium* cells in the (A) control, (B) 10 μM AgNPs, (C) 1 μM Ag^+, (D) 10 μM AgNPs + 1 μM Ag^+, (E) 10 μM AgNPs + 10 μM Ag^+, (F) 100 mg/L 2,4-DCP, and (G) 100 μM AgNPs treatments for 24 h.

clearly observed in Fig. 7C and D, and obvious Ag peaks were observed in the EDX spectra of the bright spots. The crystallography of the nanoscale Ag particles was investigated by XRD and characteristic peaks at 38° corresponded to the (111) crystal plane of the cubic AgNPs (Fig. S4). The reason for only a weak peak in the XRD pattern was probably due to the relatively low doses of AgNPs in tested samples (Chen et al., 2006). It has been reported that Ag^+ can be reduced to nanoscale Ag^0 through a biological method using enzymes, reducing sugars, and humic acid produced by microbes (Zuo et al., 2015; Vigneshwaran et al., 2006; Hebbalalu et al., 2013). Accordingly, the Ag nanoparticles in *P. chrysosporium* could originate from the added or biosynthesized AgNPs. Likewise, STEM analysis of Ag^+-treated fungi was conducted, but no bright spots were detected (data not shown), which ruling out the biosynthesis of AgNPs via the reduction of Ag^+. In addition, sizes and shapes of the bright dots were roughly consistent with those of as-prepared AgNPs, expounding the stability of AgNPs during the transport process (Huang et al., 2017). Although low solubility of AgNPs was previously shown, their internalization led to relatively high localized concentrations of released Ag^+ in small-size cells. These results indicated that in addition to AgNPs themselves, exerting a "particle-specific" effect, the dissolved Ag^+ within cells could

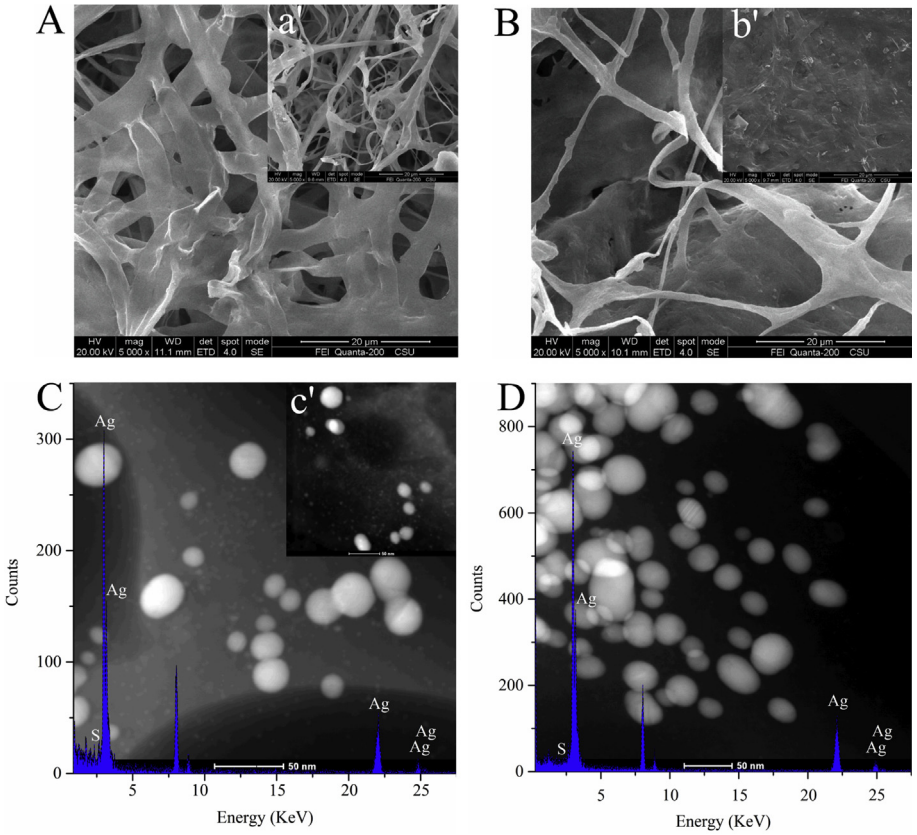

Fig. 7. SEM images of freeze-dried fungal pellets treated with (A) 10 μM AgNPs + 1 μM Ag^+, (a') 1 μM Ag^+, (B) 10 μM AgNPs + 10 μM Ag^+, and (b') 10 μM Ag^+; HAADF-STEM characterization and EDX profiles of fungal pellets from AgNPs/Ag^+-treated samples: (C) 10 μM AgNPs + 1 μM Ag^+, (c') 10 μM AgNPs, and (D) 10 μM AgNPs + 10 μM Ag^+.

Table 1
Zeta potentials (mV) of the tested solutions of AgNPs/Ag^+ alone and combinations of AgNPs and Ag^+.

Time (h)	AgNPs (μM)		10 μM AgNPs + Ag^+		Ag^+ (μM)		
	10	20	1 μM Ag^+	10 μM Ag^+	1	10	20
0	−18.0 ± 0.5	−21.3 ± 1.7	−14.3 ± 1.4	−13.7 ± 0.9	−7.7 ± 1.8	−4.0 ± 2.3	−1.3 ± 0.8
12	−31.8 ± 1.9	−25.5 ± 1.3	−27.3 ± 1.3	−23.5 ± 0.6	−28.8 ± 0.6	−24.4 ± 2.5	−20.5 ± 0.9
24	−32.0 ± 1.2	−30.6 ± 0.9	−28.6 ± 0.6	−24.4 ± 1.8	−29.0 ± 1.1	−24.5 ± 1.1	−22.8 ± 1.5
36	−34.2 ± 3.6	−33.1 ± 0.5	−27.5 ± 0.9	−25.2 ± 1.7	−28.3 ± 0.6	−25.0± 1.4	−22.2 ± 1.9

contribute to AgNP-induced cytotoxicity. Further studies on internalized Ag^+ must be conducted to determine the proportion of antimicrobial activity of Ag^+ with respect to the "particle-specific" toxicity.

It is worth noting that an increase in the number of bright spots was elicited with the increasing Ag^+ concentrations under AgNP stress, probably because Ag^+ caused more damage to membrane structures, in agreement with observations regarding biomass, plasma membrane integrity loss, and SEM. It resulted in easier penetration into cells and long-term durability of AgNPs in *P. chrysosporium*, and then "particle-specific" toxic effects of AgNPs were enhanced.

In a word, the introduction of Ag^+ not only altered cellular growth, surface morphology, and membrane structures of *P. chrysosporium* negatively, but also potentiated the "particle-specific" cytotoxicity of AgNPs.

4. Conclusion

Under the stress of 2,4-DCP and AgNPs, increased oxalate accumulation was accompanied by higher activities of MnP and LiP. EPS and extracellular proteins were elevated to cope with toxicant-induced oxidative stress. However, the production of the extracellular secretions was all inhibited to some extent as a result of Ag^+ incorporation into AgNPs in contrast to AgNPs alone. Besides the response of extracellular secretions to the stress of Ag^+ incorporation into AgNPs, SEM, HAADF-STEM, and EDX data indicated that the toxicity on *P. chrysosporium* exerted by AgNPs originated from the added nanoparticles themselves, rather than from the biosynthesis of AgNPs via reduction of Ag^+. Direct evidence of enhanced "particle-specific", concentration-dependent cytotoxicity of AgNPs caused by Ag^+ addition was also observed. This was supported by the loss of plasma membrane integrity and morphological abnormality. These findings provided new insights into the potential toxic effects of nanoparticles when combined with other chemicals, which may shed light on a more comprehensive understanding of the bioeffects of nanoparticles in complex aqueous systems.

Acknowledgements

This work was financially supported by the National Natural Science Foundation of China (51579099, 51521006 and 51508186),

the Program for Changjiang Scholars and Innovative Research Team in University (IRT-13R17), and the Hunan Provincial Natural Science Foundation of China (2016JJ3076).

Appendix A. Supplementary data

Supplementary data related to this article can be found at https://doi.org/10.1016/j.chemosphere.2017.12.185.

References

Barik, A.J., Gogate, P.R., 2017. Degradation of 2,4-dichlorophenol using combined approach based on ultrasound, ozone and catalyst. Ultrason. Sonochem. 36, 517–526.

Chen, A., Shang, C., Zeng, G., Chen, G., Shao, J., Zhang, J., Huang, H., 2015. Extracellular secretions of *Phanerochaete chrysosporium* on Cd toxicity. Int. Biodeterior. Biodegrad. 105, 73–79.

Chen, A., Zeng, G., Chen, G., Liu, L., Shang, C., Hu, X., Lu, L., Chen, M., Zhou, Y., Zhang, Q., 2014. Plasma membrane behavior, oxidative damage, and defense mechanism in *Phanerochaete chrysosporium* under cadmium stress. Process Biochem. 49, 589–598.

Chen, G.Q., Zou, Z.J., Zeng, G.M., Yan, M., Fan, J.Q., Chen, A.W., Yang, F., Zhang, W.J., Wang, L., 2011. Coarsening of extracellularly biosynthesized cadmium crystal particles induced by thioacetamide in solution. Chemosphere 83, 1201–1207.

Chen, M., Wang, L.Y., Han, J.T., Zhang, J.Y., Li, Z.Y., Qian, D.J., 2006. Preparation and study of polyacryamide-stabilized silver nanoparticles through a one-pot process. J. Phys. Chem. B 110, 11224–11231.

Cheng, Y., He, H., Yang, C., Zeng, G., Li, X., Chen, H., Yu, G., 2016. Challenges and solutions for biofiltration of hydrophobic volatile organic compounds. Biotechnol. Adv. 34, 1091–1102.

Fan, T., Liu, Y., Feng, B., Zeng, G., Yang, C., Zhou, M., Zhou, H., Tan, Z., Wang, X., 2008. Biosorption of cadmium(II), zinc(II) and lead(II) by *Penicillium simplicissimum*: isotherms, kinetics and thermodynamics. J. Hazard Mater. 160, 655–661.

Geyik, A.G., Çeçen, F., 2016. Exposure of activated sludge to nanosilver and silver ion: inhibitory effects and binding to the fractions of extracellular polymeric substances. Bioresour. Technol. 211, 691–697.

Girilal, M., Krishnakumar, V., Poornima, P., Kalaichelvan, P.T., 2015. A comparative study on biologically and chemically synthesized silver nanoparticles induced Heat Shock Proteins on fresh water fish *Oreochromis niloticus*. Chemosphere 139, 461–468.

Hatvani, N., Mécs, I., 2003. Effects of certain heavy metals on the growth, dye decolorization, and enzyme activity of *Lentinula edodes*. Ecotoxicol. Environ. Saf. 55, 199–203.

He, D., Miller, C.J., Waite, T.D., 2014. Fenton-like zero-valent silver nanoparticle-mediated hydroxyl radical production. J. Catal. 317, 198–205.

He, K., Chen, G., Zeng, G., Huang, Z., Guo, Z., Huang, T., Min, M., Shi, J., Hu, L., 2017. Applications of white rot fungi in bioremediation with nanoparticles and biosynthesis of metallic nanoparticles. Appl. Microbiol. Biotechnol. 101, 4853–4862.

He, W., Zhou, Y.T., Wamer, W.G., Boudreau, M.D., Yin, J.J., 2012. Mechanisms of the pH dependent generation of hydroxyl radicals and oxygen induced by Ag nanoparticles. Biomaterials 33, 7547–7555.

Hebbalalu, D., Lalley, J., Nadagouda, M.N., Varma, R.S., 2013. Greener techniques for the synthesis of silver nanoparticles using plant extracts, enzymes, bacteria, biodegradable polymers, and microwaves. ACS Sustainable Chem. Eng 1, 703–712.

Huang, D., Qin, X., Xu, P., Zeng, G., Peng, Z., Wang, R., Wan, J., Gong, X., Xue, W., 2016. Composting of 4-nonylphenol-contaminated river sediment with inocula of *Phanerochaete chrysosporium*. Bioresour. Technol. 221, 47–54.

Huang, D.L., Wang, C., Xu, P., Zeng, G.M., Lu, B.A., Li, N.J., Huang, C., Lai, C., Zhao, M.H., Xu, J.J., Luo, X.Y., 2015a. A coupled photocatalytic-biological process for phenol degradation in the *Phanerochaete chrysosporium*-oxalate-Fe_3O_4 system. Int. Biodeterior. Biodegrad. 97, 115–123.

Huang, D.L., Zeng, G.M., Feng, C.L., Hu, S., Jiang, X.Y., Tang, L., Su, F.F., Zhang, Y., Zeng, W., Liu, H.L., 2008. Degradation of lead-contaminated lignocellulosic waste by *Phanerochaete chrysosporium* and the reduction of lead toxicity. Environ. Sci. Technol. 42, 4946–4951.

Huang, D.L., Zeng, G.M., Feng, C.L., Hu, S., Zhao, M.H., Lai, C., Zhang, Y., Jiang, X.J., Liu, H.L., 2010. Mycelial growth and solid-state fermentation of lignocellulosic waste by white-rot fungus *Phanerochaete chrysosporium* under lead stress. Chemosphere 81, 1091–1097.

Huang, Z., Chen, G., Zeng, G., Chen, A., Zuo, Y., Guo, Z., Tan, Q., Song, Z., Niu, Q., 2015b. Polyvinyl alcohol-immobilized *Phanerochaete chrysosporium* and its application in the bioremediation of composite-polluted wastewater. J. Hazard Mater. 289, 174–183.

Huang, Z., Chen, G., Zeng, G., Guo, Z., He, K., Hu, L., Wu, J., Zhang, L., Zhu, Y., Song, Z., 2017. Toxicity mechanisms and synergies of silver nanoparticles in 2,4-dichlorophenol degradation by *Phanerochaete chrysosporium*. J. Hazard Mater. 321, 37–46.

Krystosiak, P., Tomaszewski, W., Megiel, E., 2017. High-density polystyrene-grafted silver nanoparticles and their use in the preparation of nanocomposites with antibacterial properties. J. Colloid Interface Sci. 498, 9–21.

Li, C.C., Wang, Y.J., Dang, F., Zhou, D., 2016. Mechanistic understanding of reduced AgNP phytotoxicity induced by extracellular polymeric substances. J. Hazard Mater. 308, 21–28.

Li, N., Zeng, G., Huang, D., Huang, C., Lai, C., Wei, Z., Xu, P., Zhang, C., Cheng, M., Yan, M., 2015. Response of extracellular carboxylic and thiol ligands (oxalate, thiol compounds) to Pb^{2+} stress in *Phanerochaete chrysosporium*. Environ. Sci. Pollut. Res. 22, 12655–12663.

Li, N.J., Zeng, G.M., Huang, D.L., Hu, S., Feng, C.L., Zhao, M.H., Lai, C., Huang, C., Wei, Z., Xie, G.X., 2011. Oxalate production at different initial Pb^{2+} concentrations and the influence of oxalate during solid-state fermentation of straw with *Phanerochaete chrysosporium*. Bioresour. Technol. 102, 8137–8142.

Mendes, L.A., Maria, V.L., Scott-Fordsmand, J.J., Amorim, M.J.B., 2015. Ag nanoparticles (Ag NM300K) in the terrestrial environment: effects at population and cellular level in *Folsomia candida* (Collembola). Int. J. Environ. Res. Publ. Health 12, 12530–12542.

Sheng, G.P., Xu, J., Luo, H.W., Li, W.W., Li, W.H., Yu, H.Q., Xie, Z., Wei, S.Q., Hu, F.C., 2013. Thermodynamic analysis on the binding of heavy metals onto extracellular polymeric substances (EPS) of activated sludge. Water Res. 47, 607–614.

Sheng, Z., Liu, Y., 2017. Potential impacts of silver nanoparticles on bacteria in the aquatic environment. J. Environ. Manage 191, 290–296.

Shi, Y., Huang, J., Zeng, G., Gu, Y., Chen, Y., Hu, Y., Tang, B., Zhou, J., Yang, Y., Shi, L., 2017. Exploiting extracellular polymeric substances (EPS) controlling strategies for performance enhancement of biological wastewater treatments: an overview. Chemosphere 180, 396–411.

Tang, L., Zeng, G.M., Shen, G.L., Li, Y.P., Zhang, Y., Huang, D.L., 2008. Rapid detection of picloram in agricultural field samples using a disposable immunomembrane-based electrochemical sensor. Environ. Sci. Technol. 42, 1207–1212.

Vigneshwaran, N., Kathe, A.A., Varadarajan, P.V., Nachane, R.P., Balasubramanya, R.H., 2006. Biomimetics of silver nanoparticles by white rot fungus, *Phaenerochaete chrysosporium*. Colloids Surf. B 53, 55–59.

Wang, Y.W., Tang, H., Wu, D., Liu, D., Liu, Y.F., Cao, A.N., Wang, H.F., 2016. Enhanced bactericidal toxicity of silver nanoparticles by the antibiotic gentamicin. Environ. Sci. Nano 3, 788–798.

Wang, Z., Liu, S., Ma, J., Qu, G., Wang, X., Yu, S., He, J., Liu, J., Xia, T., Jiang, G.B., 2013. Silver nanoparticles induced RNA polymerase-silver binding and RNA transcription inhibition in erythroid progenitor cells. ACS Nano 7, 4171–4186.

Xiu, Z.M., Zhang, Q.B., Puppala, H.L., Colvin, V.L., Alvarez, P.J.J., 2012. Negligible particle-specific antibacterial activity of silver nanoparticles. Nano Lett. 12, 4271–4275.

Xu, P., Leng, Y., Zeng, G., Huang, D., Lai, C., Zhao, M., Wei, Z., Li, N., Huang, C., Li, F., Cheng, M., 2015. Cadmium induced oxalic acid secretion and its role in metal uptake and detoxification mechanisms in *Phanerochaete chrysosporium*. Appl. Microbiol. Biotechnol. 99, 435–443.

Xu, P., Zeng, G.M., Huang, D.L., Feng, C.L., Hu, S., Zhao, M.H., Lai, C., Wei, Z., Huang, C., Xie, G.X., Liu, Z.F., 2012. Use of iron oxide nanomaterials in wastewater treatment: a review. Sci. Total Environ. 424, 1–10.

Yang, C., Chen, H., Zeng, G., Yu, G., Luo, S., 2010. Biomass accumulation and control strategies in gas biofilters. Biotechnol. Adv. 28, 531–540.

Yuan, X., Wang, H., Wu, Y., Zeng, G., Chen, X., Leng, L., Wu, Z., Li, H., 2016. One-pot self-assembly and photoreduction synthesis of silver nanoparticle-decorated reduced graphene oxide/MIL-125(Ti) photocatalyst with improved visible light photocatalytic activity. Appl. Organomet. Chem. 30, 289–296.

Yue, Z.B., Li, Q., Li, C., Chen, T., Wang, J., 2015. Component analysis and heavy metal adsorption ability of extracellular polymeric substances (EPS) from sulfate reducing bacteria. Bioresour. Technol. 194, 399–402.

Zeng, G., Chen, M., Zeng, Z., 2013. Risks of neonicotinoid pesticides. Science 340, 1403.

Zeng, G., Yu, M., Chen, Y., Huang, D., Zhang, J., Huang, H., Jiang, R., Yu, Z., 2010. Effects of inoculation with *Phanerochaete chrysosporium* at various time points on enzyme activities during agricultural waste composting. Bioresour. Technol. 101, 222–227.

Zhan, T., Tan, Z., Tian, X., Hou, W., 2017. Ionic liquid functionalized graphene oxide-Au nanoparticles assembly for fabrication of electrochemical 2,4-dichlorophenol sensor. Sens. Actuators B 246, 638–646.

Zhang, L., Yuan, X., Wang, H., Chen, X., Wu, Z., Liu, Y., Gu, S., Jiang, Q., Zeng, G., 2015. Facile preparation of $Ag/AgVO_3$/BiOCl composite and its enhanced photocatalytic behavior for methylene blue degradation. RSC Adv 5, 98184–98193.

Zuo, Y., Chen, G., Zeng, G., Li, Z., Yan, M., Chen, A., Guo, Z., Huang, Z., Tan, Q., 2015. Transport, fate, and stimulating impact of silver nanoparticles on the removal of Cd (II) by *Phanerochaete chrysosporium* in aqueous solutions. J. Hazard Mater. 285, 236–244.